Geophysical Research Letters

Supporting Information for

Flow strength of wet quartzite in steady-state dislocation creep regimes

Lucy X. Lu, Dazhi Jiang[a]

Department of Earth Sciences, Western University, London Ontario, Canada N6A 5B7

[a]State Key Laboratory of Continental Dynamics, Department of Geology, Northwest University, Xi'an 710069, China

Contents of this file

Introduction

A detailed description of the selection criteria of previous creep experiments for our analysis and the dataset of 19 creep experiments on quartz samples are given in supplementary information. Additionally, more detailed descriptions of the determination of tow flow laws and the self-consistent micromechanics-based homogenization approach are available in this supplementary information.

Text S1.

A total of 19 creep experiments, deformed from 700 ℃ to 1200 ℃ and corresponding to steady-state regimes 2 and 3 dislocation creep, on quartz samples are analyzed in this paper. To minimize complications from the effect of water on quartz, we only include data from samples with 0.1-0.4 wt.% H_2O added, following Tokle et al. (2019). Dislocation creep is grainsize-independent, whereas other deformation mechanisms, like grain boundary sliding and diffusion, are sensitive to the grainsize. To diminish the contributions of other mechanisms, we exclude ultrafine-grained samples (Rutter and Brodie, 2004; Fukuda et al., 2018; Richter et al., 2018) and only use samples with grainsize between 20-200 μm. These creep experiments were performed in either uniaxial compression or general shear setup. For the general shear experiments, the shear stresses (τ) and the shear strain rates ($\dot{\gamma}$) were converted to von Mises equivalent stresses ($\sigma_{eqv} = \sqrt{3}\tau$) and equivalent strain rates ($\dot{\varepsilon}_{eqv} = \frac{\dot{\gamma}}{\sqrt{3}}$) so that the results could be directly compared with those from uniaxial compression experiments where the differential stresses and axial strain rates were used. Tokle et al. (2019) have shown that converting the shear stresses and shear strain rates to von Mises equivalent stresses and equivalent strain rates causes no systematic difference between the uniaxial compression experiments and general shear experiments. The experiments we used in this paper were conducted in the Griggs-type apparatus with solid salt assemblies, molten salt, or gas confining media. The stress calibration of Holyoke and Kronenberg (2010) for Griggs apparatus with solid medium or molten-salt medium was not applied for the following three reasons: First, it is not clear yet if such stress calibration, which was determined under uniaxial compression experiments, is applicable to general shear experiments (Tokle et al., 2019). Second, Holyoke and Kronenberg (2010) pointed out that applying their calibration for molten-salt medium to the data of Gleason and Tullis (1995) only changed the fitting term A (form $1.1\times10^{-4}\,\mathrm{MPa^{-n}s^{-1}}$ to $5.1\times10^{-4}\,\mathrm{MPa^{-n}s^{-1}}$) but not the values of n or Q substantially. Third, some experimental studies suggested that this stress calibration might be overdone (Kidder et al., 2016; Richter et al., 2016), an observation consistent with our recent results (Lu and Jiang, 2019).

Data Set S1. A Dataset of 19 Creep Experiments on Quartz Samples.

	Sample	Sample ID	Stress (MPa)	Strain Rate (s^{-1})	Temperature (°C)	Confining Pressure (GPa)	Notes	Apparatus
Kronenberg & Tullis (1984)	Arkansas Novaculite 1-60μm	NV-16	250	1.60E-06	800	1.59	0.4wt% water added, stress determined at 20% strain	Griggs-type solid medium apparatus
		NV-46	280	1.60E-06	800	1.22		(NaCl, $CaCO_3$)
		NV-36	330	1.60E-06	800	0.82		
Koch et al. (1989)	Simpson Orthoquartzite 0.21±0.01mm	K874	582	1.52E-06	800	0.95		Griggs-type solid medium apparatus
		K875a	445	1.52E-06	770	1.05		
		K875b	1166	1.75E-05	770	1.03		
		K875c	176	2.11E-07	770	1.04		
		K875d	356	1.99E-06	770	1.03		
		K903	338	1.81E-06	850	0.91		
		K904a	595	1.61E-05	850	1.03		
		K904b	155	2.05E-07	850	1.04		
		K905	230	1.83E-06	850	1.07		
		K908	500	2.20E-05	875	1.27		

		K909	224	1.51E-06	900	1.16		
		K910	251	2.19E-06	900	1.16		
		K911	871	1.59E-04	900	1.14		
		K912a	87	1.48E-07	900	1.2		
		K912c	291	1.63E-06	850	1.21		
		K912d	155	2.17E-07	850	1.2		
		K919a	421	1.64E-06	750	0.94		
		K919b	212	1.87E-07	750	0.91		
		K922a	326	1.64E-06	800	1.05		
		K922b	117	1.25E-07	800	1.07		
		K922C	1138	1.86E-05	800	1.07		
		K923	472	1.82E-05	900	1.18		
		K924	927	1.90E-05	800	1.2		
		K929a	200	1.73E-06	900	1.2		
		K929b	56	2.46E-07	900	1.2		
		K929c	505	1.90E-05	900	1.2		
		K932a	800	1.44E-04	900	1.25		
		K932b	1326	1.64E-04	800	1.25		
		K933a	530	1.65E-06	750	1.15		
		K933b	225	1.57E-07	750	1.15		
		K933c	1315	1.64E-05	750	1.13		

		K934	180	1.80E-06	900	1.2		
		K936	485	1.69E-05	850	1.24		
		K938	416	1.74E-05	900	1.17		
		K939	680	2.32E-05	850	1.15		
Luan & Paterson (1992)	Silicic acid 20-30μm	5417a	350	6.00E-05	1027	0.3		Griggs-type gas medium apparatus
		5417b	500	3.00E-04	1027	0.3		
		5424	300	5.80E-05	1027	0.3		
		5433a	360	7.50E-05	1027	0.3		
		5433b	290	3.50E-05	1027	0.3		
		5433c	544	3.50E-04	1027	0.3		
		5485a	380	5.10E-05	1027	0.3		
		5485b	182	1.00E-05	1027	0.3		
		5485c	350	1.00E-04	1027	0.3		
		5490a	423	5.30E-05	1027	0.3		
		5490b	130	5.00E-06	1027	0.3		
		5490c	180	1.00E-05	1027	0.3		
		5490d	220	2.00E-05	1027	0.3		
		5490e	260	4.00E-05	1027	0.3		
		5490f	300	8.00E-05	1027	0.3		
		5490g	380	2.20E-04	1027	0.3		

		5490h	445	4.00E-04	1027	0.3		
		5493	280	5.70E-05	1027	0.3		
		5568a	160	1.00E-05	1027	0.3		
		5568b	260	1.00E-04	1027	0.3		
		5568c	205	1.20E-05	927	0.3		
		5568d	320	1.10E-04	927	0.3		
		5574a	149	1.00E-05	1027	0.3		
		5574b	238	4.30E-05	1027	0.3		
		5574c	320	1.20E-04	1027	0.3		
		5575a	270	1.00E-05	927	0.3		
		5575b	150	1.00E-05	1027	0.3		
		5575c	450	1.00E-04	927	0.3		
		5575d	295	1.00E-04	1027	0.3		
		5577a	230	1.00E-05	1027	0.3		
		5577b	420	1.00E-04	1027	0.3		
		5577c	320	5.00E-05	1027	0.3		
		5578a	168	1.00E-05	1027	0.3		
		5578b	270	1.00E-04	1027	0.3		
		5578c	348	2.00E-04	1027	0.3		
		5579a	200	1.00E-05	1027	0.3		
		5579b	420	1.00E-04	1027	0.3		

		5580a	320	1.00E-05	927	0.3		
		5580b	570	1.00E-04	927	0.3		
		5581a	400	1.00E-05	827	0.3		
		5581b	705	1.00E-04	827	0.3		
		5582a	185	1.00E-05	1027	0.3		
		5582b	280	1.00E-05	927	0.3		
		5582c	400	1.00E-05	827	0.3		
		5583a	270	5.00E-05	1027	0.3		
		5583b	380	5.00E-05	927	0.3		
		5583c	490	5.00E-05	827	0.3		
Hirth & Tullis (1992)	Black Hills Quartzite 100µm	CQ-82	100	1.00E-06	900	1.5		Griggs-type solid medium apparatus
	Heavitree Quartzite 210µm	W339	290	1.00E-06	800	1.5		Griggs-type molten salt apparatus
Tullis & Wenk (1994)	Heavitree Quartzite 180-200µm	W-370	250	1.00E-06	800	1.2		Griggs-type solid medium apparatus
	Black Hills Quartzite 100-120µm	W-502	125	1.00E-06	800	1.2		Griggs-type molten salt apparatus

Gleason & Tullis (1995)	Black Hills Quartzite 100µm	W611a	84	6.31E-06	1050	1.5	samples with no melt	Griggs-type molten salt apparatus
		W611b	100	6.31E-06	1000	1.45		
		W611c	132	7.94E-06	950	1.44		
		BA96a	43	1.58E-06	1050	1.56		
		BA96b	61	1.58E-06	1000	1.54		
		BA96c	68	1.58E-06	950	1.53		
		BA96d	89	1.99E-06	900	1.5		
		BA94a	76	1.58E-06	1000	1.56		
		BA94b	109	6.31E-06	1000	1.56		
		BA94c	141	2.00E-05	1000	1.59		
		BA94d	228	7.94E-05	1000	1.6		
		BA95a	74	1.58E-06	1100	1.68		
		BA95b	110	6.31E-06	1100	1.68		
		BA95c	142	2.00E-05	1100	1.7		
		BA95d	225	7.94E-05	1100	1.7		
Post et al. (1996)	Black Hills Quartzite 100µm	W614	290	1.00E-05	900	1.69		Tullis-modified Griggs Apparatus
		W625	310	1.00E-05	900	1.72		
		W728	330	1.00E-05	900	1.6		

Stipp & Tullis (2003)	Black Hills Quartzite 100µm	W1030	207	2.00E-06	800	1.5		
		W1085	198	2.25E-06	850	1.5		
		W1049	268	2.30E-05	900	1.5		
		W1099	149	2.35E-06	900	1.5		
		W1051	189	2.40E-05	1000	1.5		
		W1024	102	2.05E-06	1000	1.5		
		W1025	87	2.10E-06	1050	1.5		
		W1119	257	2.10E-04	1100	1.5		
		W1029	130	2.45E-05	1100	1.5		
		W1022	130	6.00E-06	1100	1.5		
		W1066	60	2.25E-06	1100	1.5		
		W1126	34	2.20E-07	1100	1.5		
Stipp et al. (2006)	Black Hills Quartzite 100µm	W1172	48	2.25E-06	1000	1.5		Griggs-type molten salt apparatus
		W1142	66	2.00E-06	950	1.5		
		W1081	139	2.30E-06	900	1.5		
		W1089	177	2.40E-06	850	1.5		
		W1082	168	2.40E-06	800	1.5		
		W1140	156	2.25E-06	750	1.5		

Chernak et al. (2009)	Black Hills Quartzite	W1341	260	1.39E-05	900	1.5		Griggs-type solid medium apparatus
Holyoke & Kronenberg (2013)	Black Hills Quartzite 100µm	TMQ - 7	162	1.60E-06	800	1.6		Griggs-type solid medium apparatus
			422	1.60E-06	800	0.85		
			175	1.60E-06	800	1.56		
Kidder et al. (2016)	Black Hills Quartzite 70µm	W1341	242	2.17E-05	900	1.3		Griggs-type solid medium apparatus
		W1505	100	1.70E-06	900	1.3		
		W1509a	120	1.60E-06	900	1.3		
		W1510	87	2.27E-06	900	1.3		
		W1525a	94	1.69E-06	900	1.3		
		W1525b	192	4.50E-05	900	1.3		
		W1526a	337	1.68E-05	900	1.3		
		W1526b	124	2.30E-06	900	1.3		
		W1518b	58	2.20E-06	900	1.3		
Heilbronner & Tullis (2002)	Black Hills Quartzite 100µm	W872	310	1.50E-05	900	1.5		Griggs-type solid medium apparatus
		W858	180	1.50E-06	900	1.5		
		W946	364	1.73E-05	875	1.5		

		W920	165	8.66E-06	900	1.5		
		W935	182	1.73E-05	915	1.5		
Holyoke & Tullis (2006)	Black Hills Quartzite 100µm	W1105	788	2.00E-05	800	1.5	minimum strength after yield	Griggs-type solid medium apparatus
		W1106	139	2.00E-06	800	1.5		
		W1153	346	2.00E-06	745	1.5		
Heilbronner & Tullis (2006)	Black Hills Quartzite 100µm	W920	121	7.22E-06	900	1.5		Griggs-type solid medium apparatus
		W1010	182	1.14E-05	915	1.55		
		W935	208	1.14E-05	915	1.5		
		W965	191	1.16E-05	915	1.55		
Nachlas & Hirth (2015)	Silica gel (20-40µm)	W1674	242	2.89E-05	900	1		Griggs-type solid medium apparatus
		W1678	286	2.89E-05	900	1		
		W1680	251	2.89E-05	900	1		
		W1699	234	2.89E-05	900	1		
		W1700	225	2.89E-05	900	1		
		W1701	199	2.89E-05	900	1		
Tokle et al. (2013)		LT379	486	5.40E-06	800	1.5		

Richter et al. (2016)	Crushed quartz crystal <100µm	BR452	1329	1.56E-05	700	1.064		Griggs-type solid medium apparatus
Richter et al. (2018)	Crushed quartz crystal <100µm	BR383	940	1.62E-05	700	1.59	viscous regime	Griggs-type solid medium apparatus
		Br388	685	1.62E-05	800	1.53		
		Br419	880	1.62E-05	800	1.56		
		Br448	630	1.67E-05	800	1.07		
		Br412	312	1.62E-05	900	1.53		
		Br337	127	1.73E-05	1000	1.51		

Text S2.

Once the values of n, m, and V are determined, the activation energy Q can be obtained based on T stepping experimental data. To evaluate the value of Q, we first take the natural logarithm of the flow law $\dot{\varepsilon} = A f_w^m \exp\left(-\frac{Q+PV}{RT}\right)\sigma^n$ and rearrange it as $\ln(\dot{\varepsilon}) - m\ln(f_w) - n\ln(\sigma) + \frac{PV}{RT} = -\frac{Q}{RT} + \ln(A)$. For each run, we can measure the temperature (T), the confining pressure (P), the strain rate ($\dot{\varepsilon}$), and the differential stress (σ). The water fugacity f_w is determined using the state equation of water (Pitzer and Sterner, 1994), assuming the partial pressure of water is equal to the confining pressure. Plotting $-\ln(\dot{\varepsilon}) + m\ln(f_w) + n\ln(\sigma) - \frac{PV}{RT}$ versus $\frac{1}{RT}$, the value of Q is obtained by linear regression. We use the T stepping experimental data of Luan and Paterson (1992) and Gleason and Tullis (1995) to determine the value of Q for high-temperature data. The T stepping experimental data of Koch et al. (1989) is used to determine Q for low-temperature data. The results are shown in Figure.S1.

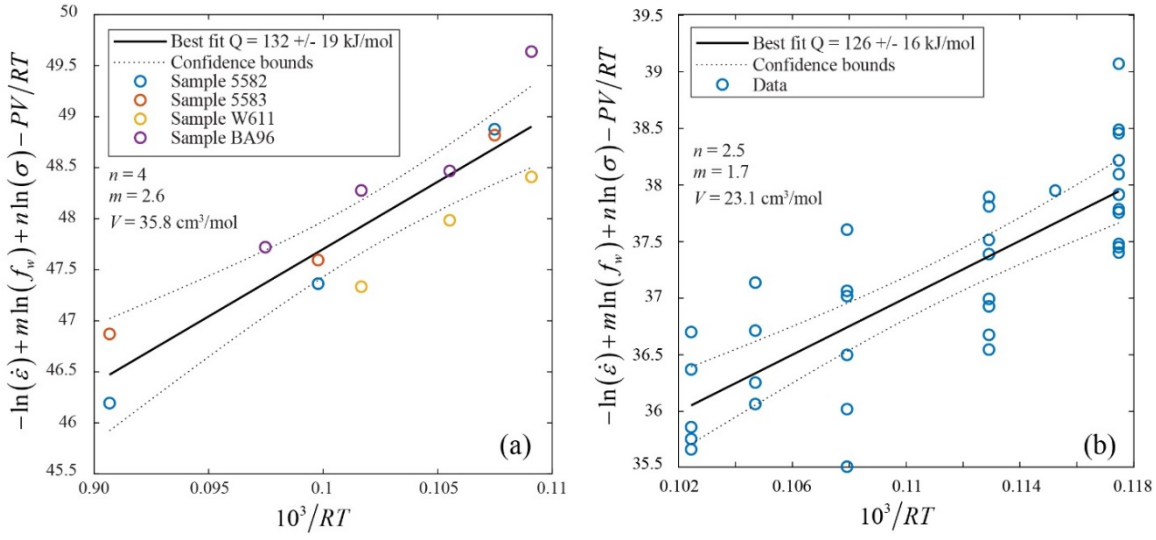

Figure S1. Plots of *T* stepping experimental data. (a). The plots of *T* stepping data of Luan and Paterson (1992; sample 5582 and sample 5583) and Gleason and Tullis (1995; sample W611 and sample BA96) using $n = 4$, $m = 2.6$, and $V = 35.8\ \mathrm{cm}^3/\mathrm{mol}$,

which yields $Q = 132 \pm 19$ kJ/mol by linear regression. (b) The plots of *T* stepping data of Koch et al. (1989) using $n = 2.5$, $m = 1.7$, and $V = 23.1$ cm^3/mol, which yields $Q = 126 \pm 16$ kJ/mol by linear regression.

Text S3.

In micromechanics, the overall rheology of quartzite is defined as the average property over a Representative Volume Element (RVE, Fig.S2), which contains a large enough number of quartz grains. When the quartzite is subjected to a remote deformation, the partitioned strain rates and stresses vary from one quartz grain to another. To evaluate the strain rate and stress in each grain, we regard a quartz grain as an ellipsoidal inclusion embedded in the matrix composed of the rest of quartz grains. The matrix is rheologically heterogeneous, but in micromechanics, it is represented by a hypothetic Homogenous Equivalent Medium (HEM, Fig.S2) whose rheology is obtained from the rheological properties of all constituent grains in an RVE. Generalized Eshelby formalism (Jiang, 2014, 2016) relates the partitioned strain rates and stresses in individual grains to the remote fields:

$$\boldsymbol{\varepsilon}_i - \mathbf{E} = \left[\mathbf{J}^{\mathrm{d}} - \mathbf{S}^{-1}\right]^{-1} : \mathbf{C}^{-1} : \left(\boldsymbol{\sigma}_i - \boldsymbol{\Sigma}\right) \tag{S1}$$

In Eq.S1, the sign "**:**" stands for the double-index contraction of two tensors. $\boldsymbol{\varepsilon}_i$ and $\boldsymbol{\sigma}_i$ are the partitioned strain rate and deviatoric stress tensors in the *i*th grain. The uppercase symbols $\mathbf{E}$ and $\boldsymbol{\Sigma}$ are the corresponding quantities in the remote field. $\mathbf{C}$ is the 4$^{\text{th}}$ order viscous stiffness (viscosity) of the matrix (HEM). $\mathbf{S}$ is the 4$^{\text{th}}$ order symmetric Eshelby tensor for each grain, and it is related to the inclusion shape and $\mathbf{C}$. The partitioned strain rates and stresses, in turn, are used to evaluate the overall strain rate ($\overline{\dot{\boldsymbol{\varepsilon}}}$) and the overall stress ($\overline{\boldsymbol{\sigma}}$) of quartzite: $\overline{\dot{\boldsymbol{\varepsilon}}} = \sum r_i \dot{\boldsymbol{\varepsilon}}_i$ and $\overline{\boldsymbol{\sigma}} = \sum r_i \boldsymbol{\sigma}_i$, where r_i is the volume fraction of *i*th grain. Numerical calculations for the self-consistent approach are realized using MATLAB scripts, the algorithms for which are in the literature (Jiang, 2014, 2016; Qu et al., 2016). The executable MATLAB files are available from authors.

As an example, we have considered a quartzite made of 500 ellipsoidal quartz grains subjected to a macroscale strain rate of 10^{-12}s^{-1}. The quartz grains have ellipsoidal

shapes with a maximum axial ratio of 2. We assume that all quartz grains are rheologically isotropic and randomly distributed; therefore, the whole quartzite is also isotropic. An individual grain follows either of the two flow laws of Eq.3. As the self-consistent homogenization method involves tensor calculations, the tensor-form flow law of quartzite is required. In order to generalize the tensor-form equation, one needs to rewrite the flow laws of the form $\dot{\varepsilon} = A f_w^m \exp\left(-\frac{Q+PV}{RT}\right)\sigma^n$ in terms of second invariants of the deviatoric stress (σ_E) and strain rate ($\dot{\varepsilon}_E$) as $\dot{\varepsilon}_E = A_i f_w^m \exp\left(-\frac{Q+PV}{RT}\right)\sigma_E^n$, where $A_i = \frac{3^{(n+1)/2}}{2} A$ (Ranalli, 1987, p.70). The tensor-form constitutive equation of isotropic materials is expressed as (Ranalli, 1987, p.70):

$$\sigma_{ij} = 2\eta_{eff}\varepsilon_{ij} \tag{S2}$$

where σ_{ij} and ε_{ij} are the components of the deviatoric stress and strain rate tensors; η_{eff} is the effective viscosity defined at a given state of stress or strain rate:

$$\eta_{eff} = \frac{1}{2} A_i^{-1} f_w^{-m} \exp\left(\frac{Q+PV}{RT}\right)\sigma_E^{1-n} \text{ or } \eta_{eff} = \frac{1}{2} A_i^{-\frac{1}{n}} f_w^{-\frac{m}{n}} \exp\left(\frac{Q+PV}{nRT}\right)\dot{\varepsilon}_E^{\left(\frac{1}{n}-1\right)} \tag{S3}$$

The effective viscosities of all quartz grains at a given state of stress or strain rate can be obtained using the parameters in two dislocation creep flow laws (Eq.3). Then numerical simulations allow us to evaluate the overall stress of quartzite with varying contributions of dominant slip systems at a given deformation condition.

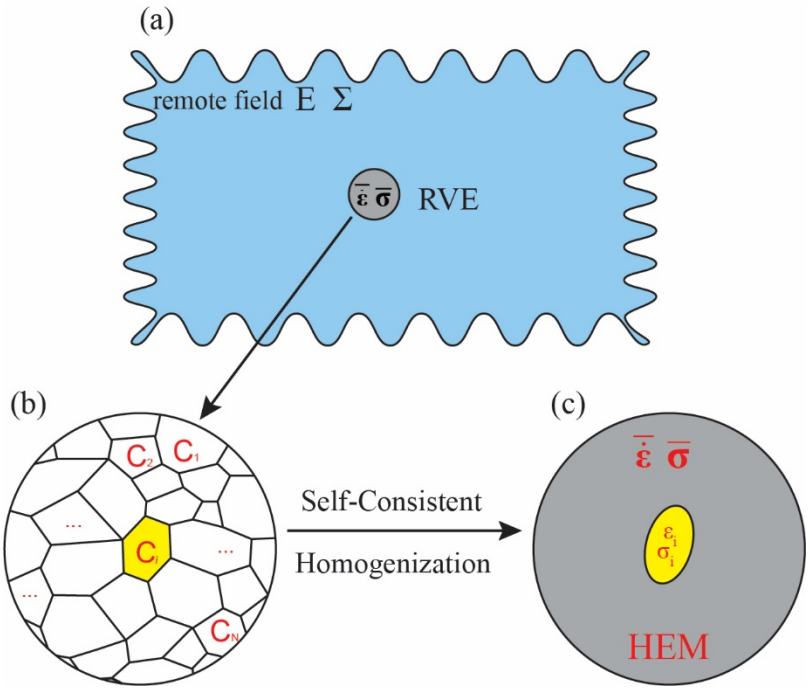

Figure S2. A conceptual diagram of the self-consistent homogenization approach. A quartzite made of *N* constituent quartz grains, denoted by $i = 1, 2, \ldots, N$, subjected to a remote deformation (a). The overall rheological property of the quartzite is defined as the average property over a Representative Volume Element (RVE) (b), which contains a large number of quartz grains. Each quartz grain is regarded as an ellipsoidal inclusion embedded in the Homogenous Effective Medium (HEM) (c), whose rheological properties are obtained from the overall rheological properties of the RVE. To get the overall rheology from the constituents' properties is called homogenization. $\boldsymbol{\varepsilon}_i$ and $\boldsymbol{\sigma}_i$ are the partitioned strain rate and deviatoric stress in a constituent grain. The uppercase symbols $\mathbf{E}$ and $\boldsymbol{\Sigma}$ are the corresponding quantities in remote field. $\overline{\dot{\boldsymbol{\varepsilon}}}$ and $\overline{\boldsymbol{\sigma}}$ are the overall strain rate and stress of the quartzite.